

Journal of Materials Chemistry C

Accepted Manuscript



This is an *Accepted Manuscript*, which has been through the Royal Society of Chemistry peer review process and has been accepted for publication.

Accepted Manuscripts are published online shortly after acceptance, before technical editing, formatting and proof reading. Using this free service, authors can make their results available to the community, in citable form, before we publish the edited article. We will replace this *Accepted Manuscript* with the edited and formatted *Advance Article* as soon as it is available.

You can find more information about *Accepted Manuscripts* in the [Information for Authors](#).

Please note that technical editing may introduce minor changes to the text and/or graphics, which may alter content. The journal's standard [Terms & Conditions](#) and the [Ethical guidelines](#) still apply. In no event shall the Royal Society of Chemistry be held responsible for any errors or omissions in this *Accepted Manuscript* or any consequences arising from the use of any information it contains.

ARTICLE

Systematic tuning the ΔE_{ST} and charge balance property of the bipolar host for low operating voltage and high power efficiency solution-processed electrophosphorescent devices

Cite this: DOI: 10.1039/x0xx00000x

Xinxin Ban^a, Wei Jiang^{*a}, Kaiyong Sun^a, Haiyong Yang^a, Yanan Miao^a, Fenghao Yang^a, Yueming Sun^{*a}, Bin Huang^a, Lian Duan^{*b}

A series of bipolar hosts based on carbazole and phenyl benzimidazole (PBI) moieties collectively named xCz-nPBI, were designed and synthesized. On the basis of different number, ratio and link-configuration of the functional groups, the influence of substitution on the chemical, photophysical and electrochemical properties of the host materials were investigated in detail. Both DFT calculation and single carrier device demonstrate that the strategy of introducing more electron-withdrawing PBI groups in the molecules can effectively enhance the electron injection and transporting ability of the bipolar host, while the increased carbazole units endow the hosts with much smaller ΔE_{ST} for efficient hole injection at the cost of sacrificing the charge balance property. As a result, the solution-processed green-emitting PHOLEDs based on Cz-6PBI shows an extremely low turn on voltage of 2.9 V, and a highest current and power efficiency of 47.8 cd A⁻¹ and 29.6 lm W⁻¹, respectively. Even at luminous as high as 1000 cd m⁻², the efficient roll-off was only 4.2%, which was far better than the 6Cz-PBI host device. Since the T₁ energy levels and triplet state locations of these hosts are similar, only the ΔE_{ST} and charge balance property should be the main factors for the EL performances. We conclude that it is not necessary to achieve too small ΔE_{ST} by introducing more carbazole moieties at the cost of weakening the electron transporting ability. As for solution-processed devices, which suffer the solvent impurities and oxygen diffusion induced strong electron trapping effect, the systemically increased electron-withdrawing PBI groups of the host materials can significantly enhance the charge balance of the emission layers (EMLs) for high power efficient solution-processed PHOLEDs.

Received 00th January 2012,
Accepted 00th January 2012

DOI: 10.1039/x0xx00000x

www.rsc.org/

1. Introduction

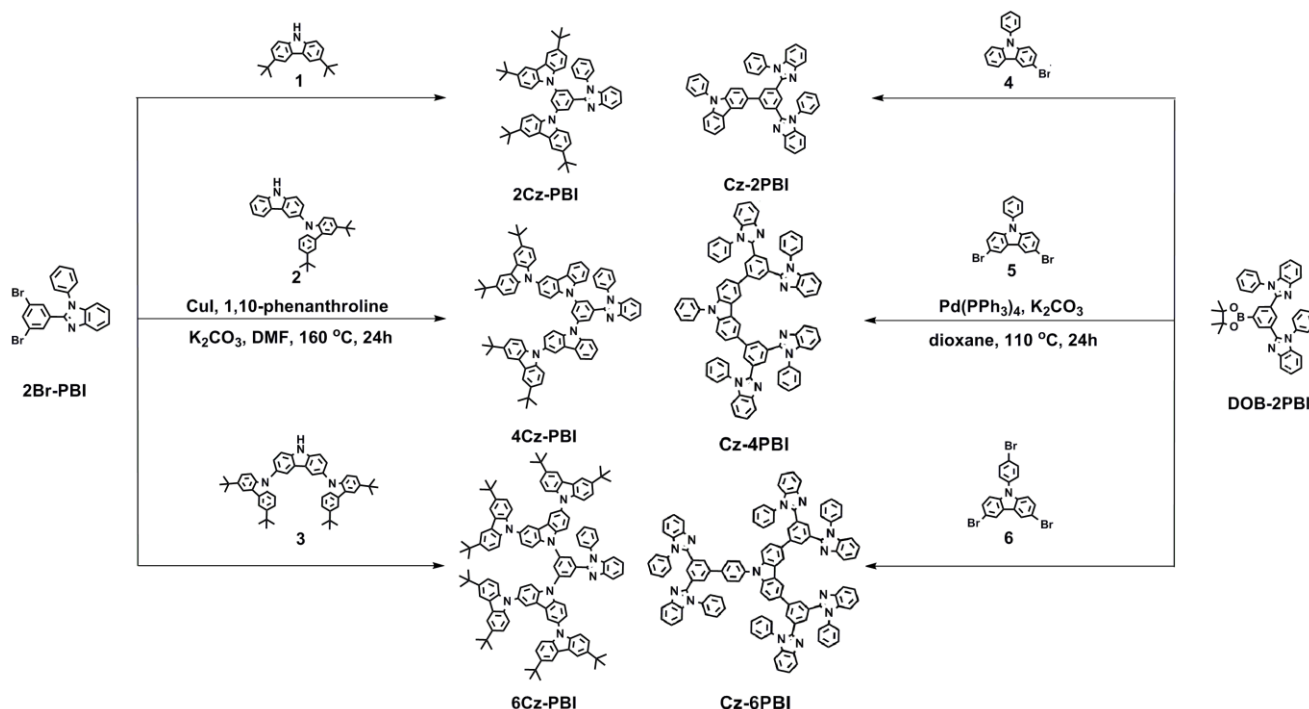
Phosphorescent organic light-emitting diodes (PHOLEDs) have attracted intense interest because of their merit of high quantum efficiency as compared to conventional fluorescent OLEDs through utilizing both singlet and triplet excitons for emission.¹ Since then, the performance of OLEDs has increased enormously especially the vacuum deposited devices with multi-active layers.² Currently, a major area of interest for PHOLEDs is large area printed lighting panels or flexible display applications, where low cost simple device structures with good efficiency are required.³ To allow for these requirements, solvent-based fabrication techniques, such as roll-to-roll or ink-jet printing, are favoured over more

expensive vacuum-based deposition techniques. Even though solution processed PHOLEDs have made considerable process in recent years, they are still a long way from commercialization.⁴ Firstly, solution processed PHOLEDs usually exhibit significant efficiency roll-off at the luminance required for practical light sources. Secondly, sequential deposition of p-doped hole-transport layer (HTL) or n-doped electron-transport layer (ETL) will be inherently difficult for the solution-processing technique, because the solvent used to deposit the subsequent layer tends to dissolve or swell the underlying layer.⁵ Finally, the major bottleneck is the relative weak device efficiency due to the solvent impurities and diffused oxygen induced electron traps.⁶

Typically, phosphorescent emitters possess longer lifetimes for further diffusion, leading to undesired concentration quenching or triplet-triplet annihilation and, thereby, declining performance.^{3b,7} To address this issue, the triplet phosphor is usually doped into an appropriate host. Thus, the key point for efficient solution-processed PHOLEDs is the development of effective soluble host materials. A good host material for solution-processed PHOLEDs should have the following features: high triplet energy to prevent reverse energy transfer from the guest to the host, good carrier transporting properties to balance the charge fluxes, appropriate orbital energy level to reduce the operation voltage, high solubility and large molecular weight to enhance the film-forming ability.⁸ Recently, great experimental efforts have focus on designing host materials with bipolar properties, since utilization of bipolar host materials can balance the charge carriers and broaden the recombination zone in the emitting layer, therefore reduce the efficiency roll-off.⁹ Another challenge to improve the performance of solution-processed PHOLEDs is reducing the operating voltage, which directly determines power efficiency of the device. In the standard PHOLEDs, the electrical carrier injection into the host material takes place on its highest occupied molecular orbital (HOMO) and lowest unoccupied molecular orbital (LUMO), that is, holes are injected into the HOMO, while electrons are injected into the LUMO. Therefore, the bipolar host material with smaller energy-gap, which correspond to the S_1 state can make the operating voltage of OLEDs lower.^{2b,10} On the other hand, for the confinement of the phosphorescent excitons, a host must have high triplet energy. Eventually, in order to achieve high power efficiency, it is necessary to adjust S_1 as low as possible while maintaining high T_1 , which is defined as small ΔE_{ST} . Su, Kido, et al. have successfully developed vacuum deposition PHOLEDs with extremely low operation voltage through bipolar host with small ΔE_{ST} .¹¹ However, the development of a promising bipolar

host material with small ΔE_{ST} , especially for solution processed PHOLEDs, is a highly challenging task due to the severe limitation of molecular design. Furthermore, the adjustment of the excited states influences both the optical and electrical properties of the host and is usually made problematic by the contradictory effects. Apart from a small ΔE_{ST} , the balanced charge carrier mobility of the host is also one of the main factors directly affecting EL performance, including the driving voltage and efficiencies.^{9e,12} To date, there is still a lack of comprehensive studies detailing the structure-performance correlation in solution-processable bipolar host. Although the high triplet energy has been proved to be an imperative advantages, some important points, such as the relationship between the ratio of hole/electron transporting moieties and the carrier injection/transporting capability, the effects of structures on the ΔE_{ST} and charge balance property, are still remain unclear.

In this study, we present an integrated investigation encompassing the thermal, chemical, photophysical and device characterization based on a series of bipolar hosts, collectively named xCz-nPBI, containing electron-transporting phenyl benzimidazole (PBI) and hole-transporting carbazole units. We choose the two moieties as building blocks since the electron-deficient 1,3,5-tris(1-phenyl-1H-benzo[d]imidazole-2-yl)benzene (TPBI) is a well-known electron-transporting and hole-blocking materials, while the electron-rich carbazole derivatives have been used extensively as hole-transporting materials for their high hole mobility. All these host materials have relatively large molecular size and high molecular weight, which enable them good film-forming ability and morphological stability during device fabrication and operation. The meta-meta configuration of the electron-donating and -accepting moieties allows these bipolar hosts to retain relatively high triplet energies. By systematically changing the proportion of electron and hole building blocks, the selective tuning of the



Scheme 1. Synthetic routes and chemical structures of xCz-nPBI.

ΔE_{ST} and the charge balance without influencing the T_1 states was successfully realized. Importantly, upon the gradually increased PBI groups, the charge balance properties of the solution-processed EMLs were extremely enhanced. As a result, Cz-6PBI supported Ir(mppy)₃-based solution-processed PHOLEDs with the extremely low turn on voltage of 2.9 V, which is among the lowest value in the solution-based green-emitting devices without p- or n-doping layer, shows the maximum current efficiency and power efficiency of 47.8 cd A⁻¹ and 29.6 lm W⁻¹, respectively. Even though the luminance reaches as high as 1000 cd m⁻², the efficiency roll-off was only 4.2%. This work suggests a new concept to overcome the drawbacks of the solution-process technology and shows the huge potential of multi-electron-transporting host in highly efficient solution-processed PHOLEDs.

2. Results and discussion

2.1 Design and Synthesis

For designing universal host materials used for solution process, an essential compromise between the triplet energy and molecular weight is inevitable, since the former requires a small conjugated length, whereas the large conjugated group benefits the latter.^{7f,13} Although we determined empirical guidelines for molecular design to achieve high T_1 in those previous studies, which require satisfying conditions of a limited conjugated length and a high excited energy group, detailed molecular design strategies to concurrently achieve small ΔE_{ST} and balanced carrier transport property, which is necessary for low driving voltage and high power efficiency, are still unclear. Commonly, carbazole is used as the repeating unit due to its sufficiently high T_1 energy and good hole transporting ability.^{3a,14} In addition, by incorporating repeating units via N-bridge connection at the 3,6-positions of phenylcarbazole will significantly increase the molecular size and thermal stability to form high-quality films by solution process, such as 4Cz-PBI and 6Cz-PBI in Scheme 1. Although it is believed that the carbazole unit does not influence the triplet excited energy levels of the molecules, the increased electron-donating moieties still have an effect on reducing carrier injection ability from the cathode and weakening the charge balance of the host. Moreover, the solution-processed emitting layer gives the devices a better hole-transporting capability and more electron traps than the vacuum-deposited layer. An effective strategy to solve this problem is the proper design of electron transport structures of the host. Thus we design and synthesis a series of bipolar hosts with different ratio of hole and electron transporting units, while maintain their high triplet energy unchanged. Improved film forming ability and morphological stability with the increased molecular weight will be expected. The selective turned ΔE_{ST} values and charge balance properties were also achieved on the basis of the reasonable combination of molecular composition and configuration. On the other hand, the relationship between the ratio of hole/electron transporting moieties and the carrier injection/transporting capability, as well as the influence of the presence of more carbazole/PBI groups on the orbital energy levels and the charge balance of the whole molecular were also focused on.

Scheme 1 illustrates the synthesis of these new compounds xCz-nPBI. The starting materials 2Br-PBI, DOB-2PBI and the other intermediates (1-6) were prepared according to the literature procedures.^{9d,6,7} 2Cz-PBI, 4Cz-PBI and 6Cz-PBI were

synthesized by Ullman coupling reaction of 2Br-PBI and the corresponding carbazole-based derivatives, whereas Cz-2PBI, Cz-4PBI, Cz-6PBI were prepared through Suzuki cross coupling reactions of DOB-2PBI with halogenated phenyl carbazole. All the target materials were further purified by silica gel chromatography before device fabrication. Their structures were fully characterized by ¹H- and ¹³C-NMR spectroscopy, mass spectrometry, and elemental analysis.

2.2 Thermal Properties

The thermal properties of these soluble bipolar hosts were investigated using thermal gravimetric analysis (TGA) and different scanning calorimetry (DSC) under a nitrogen atmosphere (Fig.1, Fig.2 and Table 1). The introduction of PBI groups to the meta-position of carbazole renders the molecule highly bulky backbone structure and non-planar, and such a molecular configuration is strongly beneficial to the thermal stability, which was indicated by their high decomposition temperatures (T_d , corresponding to 5% weight loss), in the range of 386-519 °C. The DSC curves record well-defined glass-transition temperatures (T_g) of the new compounds during the second heating scans. Along with the extension of conjugation, the T_g values of Cz-2PBI, Cz-4PBI and Cz-6PBI gradually increased to 149, 196 and 243 °C, respectively. Furthermore, compared with the corresponding Cz-nPBI series, the incorporation of high rigidity carbazole groups into xCz-PBI induced the more increased in the T_g value (198, 233 and 285 °C for x = 2, 4, 6), which are outstanding among the small molecular hosts. The high T_g values indicate steric molecular structures and weak π - π stacking, which are desirable for the soluble host materials because they can suppresses the formation of aggregates and prevent morphological changes of the amorphous organic layer upon heating. Fig.S4 gives the AFM images, showing the typical morphologies of these solution-processed thin films. As may be seen, the thin films prepared by solution process are pin-hole free and uniform with the root-mean-square roughness (RMS) less than 1 nm, which is very desirable for the further deposition of top organic layer or electrode during device preparation. It is important to note that systematically increased PBI or carbazole units both enhance the film forming property of the soluble hosts, which would facilitate charge transport and injection in the device, and improve the performance during operation.^{5e,5f}

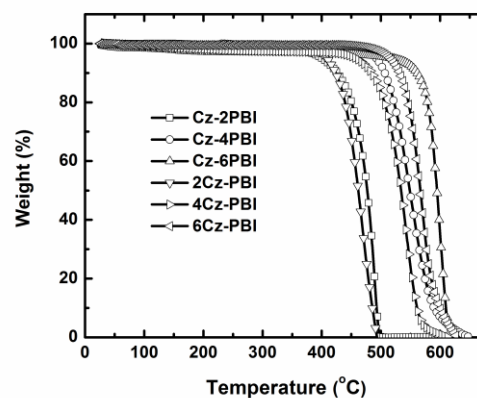


Fig.1 TGA curves of xCz-nPBI.

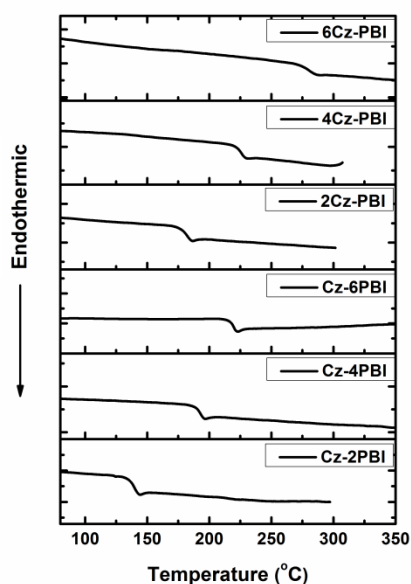


Fig.2 DSC traces of xCz-nPBI.

2.3 Photophysical Properties

The photophysical properties of these bipolar hosts were measured by UV absorption, photoluminescence (PL) and low temperature PL spectra in CH_2Cl_2 as shown in Fig.3, Fig.4 and Table 1. Due to the same active units used, the absorption peaks in the UV spectra are almost similar. The strong absorption at 236 nm can be attributed to their $\pi-\pi^*$ transitions, while the absorptions at around 291 and 305 nm are corresponding to the benzimidazole- and carbazole-centered $n-\pi^*$ transition, respectively. Compared with xCz-PBI analogues, this absorption band of Cz-nPBI becomes much stronger due to the increased proportion of PBI groups. Besides, a weak absorption band at 338 nm of the xCz-PBI series can be attributed to their ICT transition between carbazole and benzimidazole, and which was not found in the Cz-nPBI series. Therefore, both the carbazole and PBI moieties provide the main contributions to molecular excited energy levels. Moreover, it is surprising that the optical energy gaps (corresponding to the S_1 state) of xCz-PBI are remarkably reduced from 3.48 to 3.25 eV along with

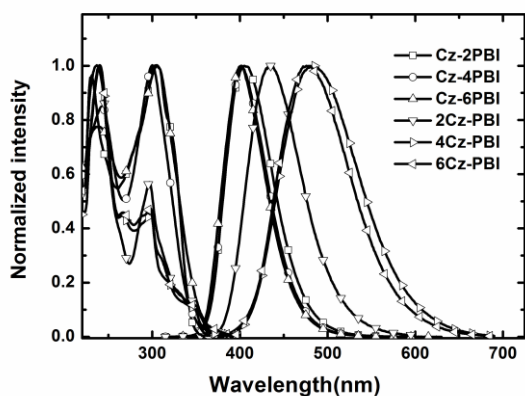


Fig.3 Normalized absorption and emission spectra of xCz-nPBI in CH_2Cl_2 .

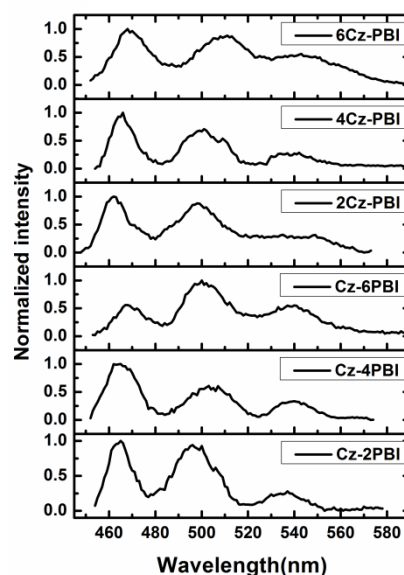


Fig.4 Phosphorescence spectra of xCz-nPBI at 77 K in CH_2Cl_2 .

the increased carbazole units, which was perfect with the DFT simulation results. The variation tendency of Cz-nPBI is the same. A more careful comparison reveals that the increased PBI moiety results in the reduction of S_1 state for 0.22 eV, while the increased carbazole group seems more effective for the absorption extension with the reduction of S_1 energy level up to 0.31 eV. Thus, through turning the ratio of the functional groups, the controllable modulation of the S_1 energy levels can be feasibly realized. In the PL spectra, xCz-PBI series exhibit significantly red-shifted emission from 435 to 478 with the increased carbazole units, which suggest that the delocalization of the excited states extend to the increased peripheral moieties. In addition, the fluorescent maxima of xCz-PBI revealed a distinct bathochromic shift from the nonpolar n-hexane to the highly polar ethanol (see Fig.S2 in the Supporting Information), which suggest that the radiative transition mechanism of them involving rapid photo-induced electron transfer between the electron donor and the electron acceptor, resulting in a large change in the dipole moment in the excited stage and a subsequent solvent relaxation process. In sharp contrast, the increased PBI units do not obviously change the emission properties of Cz-nPBI, which can be attributed to the twisted structure and the indirectly linking mode induced long distance of the donor and acceptor units. In addition, the narrowing of half peak width and the almost same PL spectra in the film state compare to those in solution reflect that the introduction of PBI units to the meta-positions of the carbazole core further render the molecule in a non-planar three-dimensional structure. Such a molecular conformation can effectively inhibit unwanted intermolecular interaction and decrease the structure-relaxation-induced excited-energy loss. The triplet energies (T_1) of Cz-nPBI and xCz-PBI were also measured from the first phosphorescent emission peak in dichloromethane at 77 K to indicate if the molecular design configuration could maintain the high T_1 states. Satisfactorily, the substitution of different ratio of carbazole and PBI moieties exhibits little effect on the T_1 energy level (around 2.68 eV), which was consisted with the value of well-known material TPBI. Hence, we conclude that the excited triplet electronic structures are dominated by the benzimidazole moiety and

Table 1 The thermal, photophysical, and electrochemical data of the compound

Host	T_g/T_d^a [°C]	RMS [nm]	λ_{abs}^b [nm]	λ_{em} [nm]	FWHM [nm]	E_T^d [eV]	E_{ox}^f [V]	HOMO ^g [eV]	LUMO ^h [eV]	S_1 [eV]	ΔE_{ST} [eV]
Cz-2PBI	143/386	0.62	318,304,230	408 ^b	64 ^b	2.67 ^d	0.81	-5.61	-2.05	3.56 ⁱ	0.89 ^d
				404 ^c	53 ^c	2.84 ^e				3.66 ^e	0.82 ^e
Cz-4PBI	196/492	0.45	299,241	403 ^b	54 ^b	2.67 ^d	0.81	-5.61	-2.15	3.46 ⁱ	0.79 ^d
				407 ^c	50 ^c	2.82 ^e				3.67 ^e	0.84 ^e
Cz-6PBI	223/519	0.39	304,238	400 ^b	51 ^b	2.66 ^d	0.84	-5.64	-2.30	3.34 ⁱ	0.68 ^d
				403 ^c	50 ^c	2.82 ^e				3.57 ^e	0.75 ^e
2Cz-PBI	186/408	0.59	345,295,235	435 ^b	72 ^b	2.68 ^d	0.66	-5.46	-1.98	3.48 ⁱ	0.80 ^d
				402 ^c	52 ^c	2.91 ^e				3.33 ^e	0.41 ^e
4Cz-PBI	233/458	0.30	335,295,267,239	484 ^b	94 ^b	2.67 ^d	0.49	-5.29	-2.01	3.28 ⁱ	0.60 ^d
				427 ^c	56 ^c	2.92 ^e				3.13 ^e	0.20 ^e
6Cz-PBI	285/510	0.30	348,296,266,239	478 ^b	98 ^b	2.66 ^d	0.46	-5.26	-2.01	3.25 ⁱ	0.57 ^d
				418 ^c	68 ^c	2.86 ^e				2.98 ^e	0.12 ^e

^a Td, corresponding to 5% weight loss. ^b Measured in CH₂Cl₂ solutions. ^c Neat film data measured at 298K. ^d Estimated from the onset of phosphorescence in the CH₂Cl₂ glass at 77K. ^e Results of the DFT calculation. ^f The onset potential of oxidation as referenced to ferrocene (Fc). ^g The HOMO energies was determined from the onset potentials for oxidation with regard to the energy level of ferrocene (4.8 eV below vacuum). ^h Calculated from the HOMO and optical energy gap. ⁱ Estimated from the absorption edges.

which was demonstrated by the DFT simulation of the triplet spin-density-distribution. Therefore, the decreased excited singlet energy (S_1) together with the maintained high triplet energy (T_1) will make the energy difference between S_1 and T_1 (so-called ΔE_{ST}) smaller, which is a positive effect on facilitating the carrier injection in the EML.

2.4 Electrochemical Properties

The bipolar electrochemical properties of these hosts were studied in solution through cyclic voltammetry (CV) using tetrabutylammonium hexafluorophosphate (TBAPF₆) as the supporting electrolyte and ferrocene as the internal standard. Fig.5 shows that all the compounds have distinct reduction and oxidation behaviors, which clearly indicate their potential in bipolar carrier transport. During the anodic sweeping in CH₂Cl₂, the cyclic voltammograms of Cz-2PBI, Cz-4PBI and Cz-6PBI showed irreversible oxidation peaks with almost the same turn-on voltage around 0.8 V, corresponding to the highest occupied molecular orbital (HOMO) energy level of -5.6 eV, while the turn-on voltage of the semi-reversible oxidation peak of 2Cz-PBI was 0.66 V, corresponding to HOMO energy levels of -5.46 eV. However, 4Cz-PBI and 6Cz-PBI underwent reversible oxidation process with relatively lower onset potentials of 0.46 and 0.49 V, corresponding to HOMO energy levels of 5.26 and 5.29 eV, respectively, which indicates that the oxidation process was facilitated upon the increased electron-donating carbazole segments in the 3,6-position. When performing cathodic scans in DMF, six bipolar compounds all underwent irreversible reduction corresponding to the benzimidazole moiety, which was demonstrated by the location of LUMOs in the DFT simulation. Although the reduction peaks were all -2.57 V, the onset voltages of Cz-2PBI and Cz-4PBI were -2.45 and -2.33 V, corresponding to the LUMO of -2.35 and -2.47 eV, respectively. As for Cz-6PBI, besides an irreversible reduction peak at about -2.46 V, the incorporate two additional PBI units induce the onset potential further shift to -2.26 V and result in a deeper LUMO of -2.54 eV. The sequential lowering of the LUMO by 0.19 eV should be ascribed to the extension of the

electron-withdrawing effect to the molecular core by banding more PBI groups. However, the situation for 2Cz-PBI, 4Cz-PBI and 6Cz-PBI was similar with the onset voltage at -2.48 V, corresponding to the LUMO of -2.32 eV, which demonstrate that more carbazole groups do not influence the LUMO distribution and the reduction sites were located on the acceptor PBI branch. Furthermore, we also calculated the LUMO energy levels from the HOMO values and the optical band gaps (E_g) by using the equation of LUMO = HOMO + E_g . The measured oxidation potentials and calculated HOMO/LUMO energies are summarized in Table 1. These CV data are precisely consistent with those from the DFT calculations.

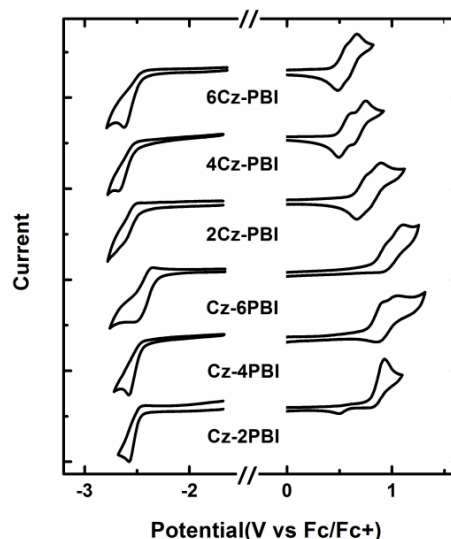


Fig.5 Cyclic voltammogram of xCP-nPBI in CH₂Cl₂ for oxidation scan, DMF for cathodic scan.

2.4 DFT simulation

To understand the nature of the optical and electrochemical properties of these bipolar hosts, the contributions of carrier transporting groups on the frontier molecular orbitals (FMOs) were systematically investigated with the density functional theory (DFT) calculations. The optimized geometries show that the carbazole and PBI units are significantly twisted to the core, resulting in a non-planar structure in each molecule. These geometrical characteristics can effectively suppress molecular recrystallization and limit the extent of conjugation between the central core and the branches, which improves the morphological stability of the thin films and keeps the triplet energy gap at a very high level of these hosts. The highest occupied molecular orbitals (HOMO) were mainly contributed by their electron-donating carbazole moieties, while their lowest unoccupied molecular orbitals (LUMO) were located on electron-withdrawing PBI units. All of the compounds have almost complete separation of the HOMO and LUMO at the hole- and electron- transporting groups, which is preferable for efficient bipolar charge transport in the host matrix. The contour plots of the FMOs are presented in Fig.6. It is shown that the LUMO of Cz-nPBI are significantly reduced with the incorporating more PBI groups, which should be attributed to the strongly electron-withdrawing effect of the substitution. Although the HOMO of Cz-6PBI is 0.02 eV larger than that of Cz-4PBI, the S_1 value of Cz-6PBI is 0.14 eV smaller. This also shows the strongly enhancement of electron injection property by the increased PBI groups. Compare with

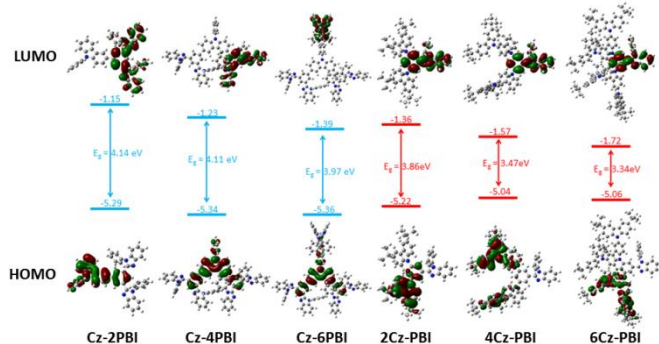


Fig.6 Energy level diagrams and molecular configuration of xCz-nPBI.

2Cz-PBI, the energy levels of the LUMO and HOMO of 4Cz-PBI remarkably decrease by 0.21 and 0.18 eV, respectively. Therefore, the introduction of carbazole groups at the C₃ positions of N-phenylcarbazole can efficiently decrease the energy gap of 4Cz-PBI. When further incorporate another two carbazole groups at C₆ position, the energy gap of 6Cz-PBI is 0.52 eV lower than that of 2Cz-PBI. This indicates that S_1 can be reduced through introduction of both hole and electron transporting groups in a chromophore. If we could simultaneously reserve T_1 of the host, the critical requirement of both high T_1 and small ΔE_{ST} can be satisfied. Hence, the triplet states of xCz-nPBI were also simulated to obtain the spin-density distributions (SDDs), which indicate the locations of the T_1 excited states. According to the contours of the SDDs (see Fig.7), the T_1 states of these hosts are mainly contributed by PBI unit, which indicates the involvement of carbazole and PBI groups in the meta-position do not influence on the molecular excited states. The calculated T_1 states are

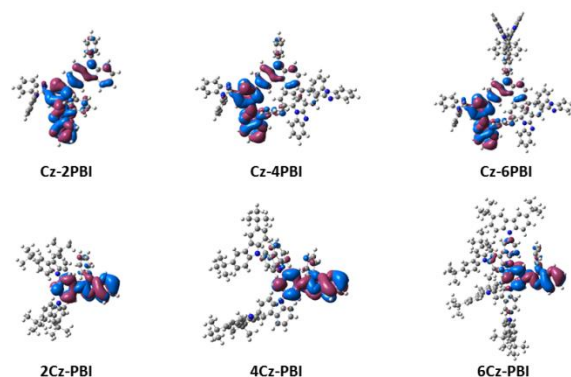


Fig.7 Spin-density distribution of the T_1 state of xCz-nPBI.

between 2.8 and 2.9 eV, which are in accord with the results estimated from the low temperature phosphorescent spectra. Therefore, in these bipolar systems, all of the building blocks have been well-managed to maintain T_1 to the greatest extent and the ΔE_{ST} value is consequently reduced from 0.84 to 0.12 eV on the basis of the reasonable combination of molecular composition and linkage modes.

As for the carrier transporting and charge balance features, the reorganization energies for both electron and hole of these hosts, which reflects the geometry relaxation energies of one molecule going from the neutral-state geometry to the charged-state geometry, were calculated at the B3LYP/6-31G(d) level. Usually, the transport of the electron or hole in the organic solid can be viewed as an electron hopping process, which can be accounted for by the Marcus electron transfer theory.^{9i,15} The intermolecular transfer of hole and electron can be represented by Eq. 1



In which, $M^{+/-}$ indicates the molecule in a cationic or anionic state. M^* is a neighboring molecule in a neutral state. If the temperature is high enough to guarantee the classical vibrational modes in the treatment, the corresponding charge-transfer rate, k_{CT} , can be described by Marcus' equation

$$k_{CT} = \frac{4\pi^2}{h} H_{AB}^2 \frac{1}{\sqrt{4\pi\lambda k_B T}} \exp\left(-\frac{\lambda}{4k_B T}\right) \quad (2)$$

Where λ is the reorganization energy, H_{AB} is the charge transfer integral (or the electronic coupling matrix element) between the relevant two molecules, and T is the temperature. The h and k_B are the Planck and Boltzmann constants, respectively. Since the intermolecular charge-transfer processes considered in OLEDs involve direct contacts in amorphous films and the range of H_{AB} is rather limited, the mobility of electrons and holes should be dominated by their respective reorganization energies λ .^[15c, 16]

Therefore, a low λ value is necessary for an efficient charge transport according to Eq. 1. Besides the reorganization energies, other related energies including ionization potentials (IP) and electron affinities (EA) were also calculated. It is generally considered that a smaller IP will contribute to a low hole-injection barrier, while a larger EA can improve the electron-injection ability from the cathode to the emitting materials. The corresponding IP, EA, $\lambda^{+/-}$ and $k^{+/-}$ are listed in Table 2. It shows that Cz-4PBI and Cz-6PBI have larger EA than Cz-2PBI, indicating that the attached PBI units are favorable for the improvement of the electron injection ability. As for IP, the carbazole unit at 3- and 6-positions also exerts a

Table 2 Reorganization energies calculated by DFT B3LYP/6-31G(d)

Host	IP _v /eV	HEP/eV	EA _v /eV	EET/eV	λ ⁺ /eV	λ ⁻ /eV	k ⁺ /k ⁻
Cz-2PBI	6.40	6.19	0.09	0.49	0.21	0.40	10.0
Cz-4PBI	6.28	6.14	0.41	0.66	0.14	0.24	4.0
Cz-6PBI	6.22	6.11	0.65	0.81	0.12	0.15	1.5
2Cz-PBI	6.24	6.14	0.18	0.76	0.10	0.58	241
4Cz-PBI	5.86	5.75	0.41	1.01	0.11	0.59	230
6Cz-PBI	5.74	5.67	0.64	1.20	0.07	0.55	280

prevented by the energy barrier between the work function of Al ($\Phi_f = 4.2$ eV) and the electron affinity (EA) of the bipolar hosts (1.9 ~ 2.3 eV for xCz-nPBI) in the hole-dominant devices. We found that the current density of their electron-only devices were proportional to the number of PBI groups and inversely proportional to the number of carbazole groups. It was shown that the increased electron-transporting benzimidazole in the Cz-4PBI and Cz-6PBI supported their devices with the strongest electron-

positive influence on the decreasing the IP values and enhancing the hole-injection ability for 4Cz-PBI and 6Cz-PBI comparing to 2Cz-PBI. These properties indicate that the introduction of electron-donating carbazole or electron-withdrawing benzimidazole would facilitate the hole- or electron-injection ability of the host, which coincides with the results of FMOs and electrochemical experiment. However, compounds with more carbazole groups (like 2Cz-PBI, 4Cz-PBI and 6Cz-PBI) all have much larger λ^- values (about 0.58, 0.59, and 0.55 eV, respectively) compared with Cz-nPBI series whose λ^- values are approximately below 0.4 eV. Combining the relationships between charge transporting abilities and the values of λ , it is easy to draw a conclusion that the electron transporting properties of these hosts are weakened severely by the introduction of more electron-rich carbazole units. Furthermore, the increased proportion of carbazole units in the molecule simultaneously enhance the hole transporting ability of 6Cz-PBI with the extremely low λ^+ value of 0.07 eV, which induces the hole-transporting rate 280 times higher than that of electron. Thus, even though 4Cz-PBI and 6Cz-PBI perform well in the carrier injection ability, the charge balance property is poorer as seen from the hole and electron reorganization. In contrast, the increased PBI not only improve the electron transporting ability but also keeps the value of λ^+ as low as 0.12 eV, especially Cz-6PBI which has the comparative λ^+ and λ^- values indicate the similar hole- and electron-transporting rate and excellent charge balance.

In this sense, we successfully and selectively enhanced the carrier-injecting/transporting ability of xCz-PBI and Cz-nPBI with only small influences on T_1 excited energy levels. More importantly, DFT calculations reflected that although the 3,6-position substituted carbazole derivatives are superior in carrier injection with much more suitable FMOs and small ΔE_{ST} , they show somewhat inferior in maintaining the charge balance of the material. Based on these bipolar hosts, the question arises whether it is worth achieving small ΔE_{ST} with the cost of reduced charge balance property.

2.4 Single carrier devices

To further investigate the charge-injection and transport properties in PHOLEDs containing solution-processed hosts, two types of single-carrier dominant devices were fabricated, including electron-dominant devices, ITO/ solution-deposited bipolar hosts (100 nm)/Cs₂CO₃/Al, and hole-dominant devices, ITO/PEDOT:PSS/solution-deposited bipolar hosts (100 nm)/Al. It is assumed that hole-injection from the ITO can be suppressed by the large energy barrier between the work function of ITO ($\Phi_f = 4.5$ eV) and the ionization potential (IP) values of the bipolar hosts (5.3~5.6 eV for xCz-nPBI) in the electron-dominant devices. Similarly, electron injection can be

transporting ability among these hosts, which was proven by the highest electron current density. As the DFT calculations showed, although the carbazole groups can modify the FMOs to reduce the ΔE_{ST} , more peripheral groups suppress the interaction between the PBI groups, which will extremely weaken the electron transporting ability of the host. Indeed, the electron current density of 4Cz-PBI and 6Cz-PBI involved devices were dramatically decreased for several orders of magnitude compared with those of the devices based on Cz-4PBI and Cz-6PBI, which results in the worse electron-transporting performance owing to their more steric hindrance of the peripheral carbazole groups restraining the intermolecular communication between the electrically active moieties. In contrast, in the hole-only devices, the gradually increased PBI units do not severely decrease the current density of Cz-nPBI series, even though the pendant carbazole groups endow xCz-PBI series with the highest currents density.

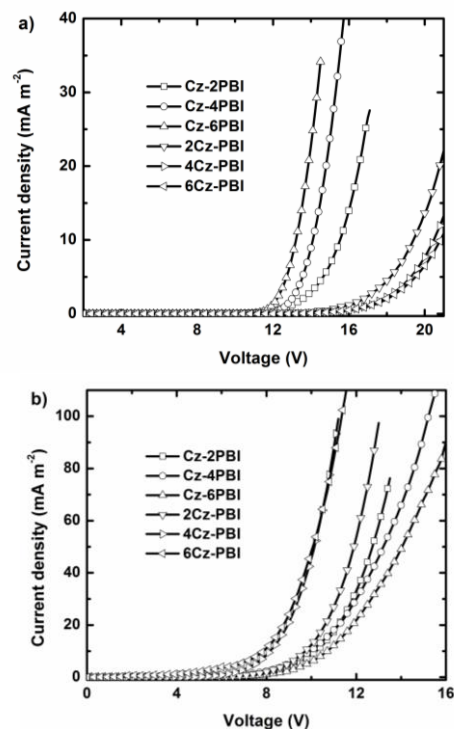


Fig.8 Current density-Voltage (J-V) characteristics of carrier-only devices: (a) electron only, (b) hole only.

Actually, the molecules in solution-processed films are not closely packed, solvent impurities and oxygen can easily diffuse into the film which could be a plausible cause for the formation of electron traps. Thus, solution processing may lead

to a reduction in the electron transport while facilitate the hole. This further indicates the importance of enhancing the electron transporting properties of the host to make the carrier transporting more balance, which is the key point to determine the location of the electron-hole recombination zone and affecting the device efficiency. In general, combining the optical, electrochemical and DFT simulations, the carrier injecting and transporting ability of the bipolar host can be systematically controlled through changing the number and ratio of the functional groups in the molecule while maintaining the excited triplet states distributing unchanged.

2.5 EL performance of the PHOLEDs

To clarify the effect of the selective modification of ΔE_{ST} and charge balance properties on the improving the EL performance of the solution-processed PHOLEDs, the green-emitting devices A-F were fabricated with the general configuration of ITO/PEDOT: PSS (40nm)/host: Ir(mppy)₃ (10 wt%, 60nm)/TPBI (40nm)/Cs₂CO₃ (1nm)/Al (100nm) by spin coating method. The schematic energy level diagram of the device is

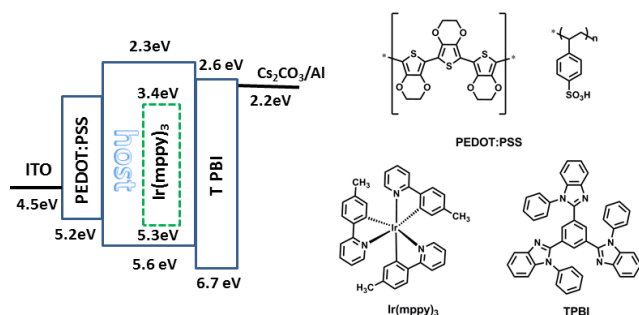


Fig.9 Structures of the materials in the devices and the energy-level diagrams.

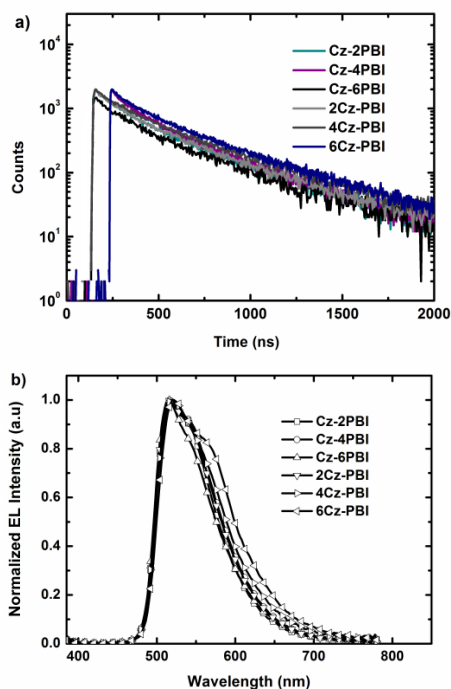


Fig.10 a) Transient photoluminescence decay curves of Ir(mppy)₃ doped films monitored at 520 nm. b) EL spectra for the devices A-F.

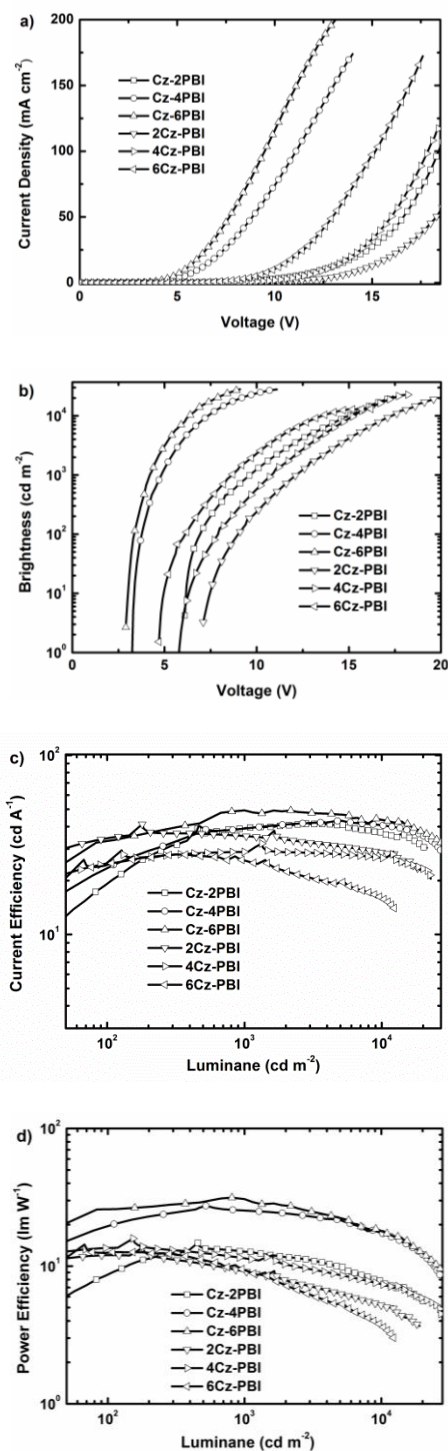


Fig.11 a) Current density-voltage (J-V) curves. b) Brightness-voltage (V-B) curves. c) Luminous efficiency as a function of brightness. d) Power efficiency as a function of brightness.

shown in Fig.9. In these devices, ITO (indium tin oxide) and Al (aluminum) served as the anode and cathode, respectively. PEDOT: PSS (poly(3,4-ethylenedioxythiophene):poly(styrene sulfonate)) and Cs₂CO₃ (caesium carbonate) were used as the hole- and electron-injection layer, respectively. TPBI (1,3,5-tris(1-phenyl-1H-benzo[d]imidazol-2-yl)benzene) was used as electron-transporting and hole-blocking material. All of these

Table 3. Device performances of the PhOLEDs

Device	Host	V_{on}	$\eta_{c,max}$	$\eta_{p,max}$	At 100cd m ⁻²	At 1000cd m ⁻²	CIE [x, y]
		[V]	[cd A ⁻¹]	[lm W ⁻¹]	[V]/[cd A ⁻¹]/[lm W ⁻¹]	[V]/[cd A ⁻¹]/[lm W ⁻¹]	
A	Cz-2BMZ	6.1	41.3	13.9	7.0/20.3/9.1	9.6/38.9/12.7	(0.31, 0.60)
B	Cz-4BMZ	3.2	44.5	28.3	3.9/27.4 /21.9	4.9/38.8/24.8	(0.31, 0.60)
C	Cz-6BMZ	2.9	47.8	29.6	3.7/32.5/27.5	4.9/45.8/29.3	(0.30, 0.60)
D	2Cz-BMZ	7.2	38.9	12.2	9.1/34.8/11.9	12.2/35.3/9.1	(0.31, 0.60)
E	4Cz-BMZ	5.7	29.6	10.5	7.9/24.8/9.8	10.9/28.8/8.3	(0.31, 0.60)
F	6Cz-BMZ	4.8	27.5	14.3	6.2/24.9/12.6	8.7/25.7/9.3	(0.32, 0.60)

devices exhibited stable green emissions attributed to Ir(mppy)₃ (Fig.10). Figure 11 shows the J-V-L characteristics and the curves of current efficiency and power efficiency versus brightness. Table 3 summarizes the electroluminescence data of the devices. The efficient energy transfer and triplet excitons confinement were demonstrated by the transient photoluminescence decays of xCz-nPBI based films doped with 10 % Ir(mppy)₃, which exhibit mono-exponential decay curves without long decay components (Fig.10). Therefore, the carrier injection and transporting in the EMLs will be the main factors to directly influence the EL performance of these devices. According to the DFT calculation and experiment results, the small ΔE_{ST} can facilitate the carrier injection, while the minimized reorganization energy will enhance the charge transporting ability. Indeed, it is shown that the current density characteristics of these devices were remarkably dependent on the electrical properties of the hosts. Significantly, owing to the stronger electron transporting ability of Cz-4PBI and Cz-6PBI, the turn on voltage of device B and C (3.2 and 2.9 V) were remarkably lower than that of other devices. Both devices exhibit high performance with a rather low efficiency roll-off at high brightness. For instance, device C exhibits maximum current efficiency of 47.8 cd A⁻¹, maximum power efficiency of 29.6 lm W⁻¹, with an efficiency roll-off of 4.2% at the luminance of 1000 cd m⁻²; while device B displays a maximum current efficiency of 44.5cd A⁻¹, maximum power efficiency of 28.3 lm W⁻¹, with an efficiency roll-off of 8.7% even at 10000 cd m⁻². These values are among the highest data for solution-processed green emitting PHOLEDs reported until now, and remarkably higher than device A and D using traditional compounds Cz-2PBI and 2Cz-PBI as hosts. However, the turn-on voltage of 5.7 V of device E was lower than the 7.2 V of device D, which can be attributed to the improved carrier injection ability of 4Cz-PBI with a relatively low ΔE_{ST} . When further minimizing the ΔE_{ST} by introducing another two carbazole groups at C₆ position of 6Cz-PBI, the distinctly decrease of the turn-on voltage was also achieved. Although the turn on voltages of device E and F were relatively lower than that of A and D, the sharp decline of efficiencies at high luminance implies the unbalanced carrier transportation in their EMLs, which should be attributed to the much stronger hole transporting ability of 4Cz-PBI and 6Cz-PBI. Furthermore, suffering from the worst electron transporting ability, device E and F showed the smallest power efficiencies (10.5 and 14.3 lm W⁻¹) compared with the analogous devices B and C. The Commission International de l'Eclairage (CIE) coordinates vary little for the devices based on the different type of host.

This could be attributed to the recombination zone shift in devices owing to the different charge transporting abilities of the hosts. The difference between the brightness of device A-F were much more distinct that Cz-4PBI and Cz-6PBI endowed their devices B and C with the much higher luminance at the same voltage compared with device E and F based on 4Cz-PBI and 6Cz-PBI, which demonstrate that the improved electron transporting property can broad the charge recombination zone and reduce the non-radiative decay pathways. Obviously, the EL performance of E and F was much worse than that of B and C, although 4Cz-PBI and 6Cz-PBI have much smaller ΔE_{ST} than those of Cz-4PBI and Cz-6PBI. Considering the similar triplet state location and T₁ energy level of these hosts, only the ΔE_{ST} and charge balance should be the main factors for the EL performances. As in the common solution-processed devices, the solvent impurities and diffused oxygen often have strong electron trapping ability,^[6b] the moderately enhanced electron transportation in the host can facilitate the charge balance in EMLs. This indicates that it is not reasonable to achieve too small ΔE_{ST} to facilitate the hole injection ability through incorporating more carbazole moieties with the cost of weakening the electron transporting ability of the hosts. For a high power efficiency and low operating voltage solution-processed PHOLEDs, an ideal soluble host should possess both balanced carrier transporting ability and suitable ΔE_{ST} for efficient charge injection.

3. Conclusions

In summary, six bipolar hosts collectively named xCz-nPBI were designed and synthesized to investigate the influence of the different ratio and position of the functional groups on their chemical and optophysical properties. The improved morphological and thermal stability was proved by AFM measurement and thermal analysis. The optical investigations showed that meta-substituted carbazole and PBI groups do not change the excited T₁ energy level of the host due to the same triplet state location, which was demonstrated by the spin-density distribution. However, the ΔE_{ST} of xCz-PBI was minimized by the increased proportion of carbazole units, which can induce the separating of the HOMO and LUMO of a molecule. Thus, the fixed T₁ and continuously turned ΔE_{ST} was successfully achieved. On the other hand, the reorganization calculations imply that the number of PBI groups and electron-transporting ability are proportional. Furthermore, the single carrier devices also prove that the increased PBI units can significantly enhance the charge balance of the hosts owing to

their improved electron-transporting property and comparable hole-transporting ability. On the basis of the green-emitting solution-processed PHOLEDs, the influences of the small ΔE_{ST} and charge balance property on the EL performances were investigated. The device using Cz-6PBI as host exhibited an ideal turn-on voltage of 2.9 V, and a maximum efficiencies of 47.8 cd A⁻¹ and 29.6 lm W⁻¹. Even as the brightness reaches 1000 cd m⁻², the efficiency roll-off was only 4.2%. Although the small ΔE_{ST} of 4Cz-PBI and 6Cz-PBI also endow their corresponding devices with a relatively lower turn on voltages, the sharp decline of efficiencies at high luminance implies the unbalanced carrier transportation in their EMLs, which should be ascribed to the worst electron transporting ability with the increased carbazole units. Therefore, when the triplet state distribution and T₁ energy levers of the hosts were similar, the balanced charge transporting behaviors seems more important than the extremely small ΔE_{ST} in the solution-processed devices. Suffering the solvent impurities and oxygen diffusion induced strong electron trapping effect, this work provided a valuable strategy for readily enhancing the charge balance of solution-processed device through increasing the number and ratio of electron transporting units. We believe that these results can trigger the insight into the charge transport phenomenon in solid state, which would establish a new guideline in molecular design of soluble materials for more power-efficient solution-processed PHOLEDs with desirable operating voltage.

4. Experimental

4.1 General information

All reactants and solvents, unless otherwise stated, were purchased from commercial sources and used as received. ¹H-NMR and ¹³C-NMR spectra were measured on a BRUKER AMX 300- or 500-MHz instrument with tetramethylsilane as the internal standard. Elemental analysis was performed on an Elementar Vario EL CHN elemental analyzer. Molecular masses were determined by a FINNIGAN LCQ Electro-Spraying Ionization-Mass Spectrometry (ESI-MS), or a BRUKER DALTONICS Matrix-assisted laser desorption-ionization time-of-flight mass spectrometry (MALDI-TOF-MS), with α -cyano-hydroxycinnamic acid as a matrix. Absorption and photoluminescence emission spectra of the target compound were measured using a SHIMADZU UV-2450 spectrophotometer and a HORIBA FLUOROMAX-4 spectrophotometer, respectively. Phosphorescence spectra at 77 K were measured in a dichloromethane solvent. Thermogravimetric analysis (TGA) was recorded with a Netzsch simultaneous thermal analyzer (STA) system (STA 409PC) under a dry nitrogen gas flow at a heating rate of 10 °C min⁻¹. Glass-transition temperature was recorded by (DSC) at a heating rate of 10 °C min⁻¹ with a thermal analysis instrument (DSC 2910 modulated calorimeter). Cyclic voltammetry (CV) was performed on a CHI750C voltammetric analyzer in CH₂Cl₂ or THF solutions at a scan rate of 100 mV s⁻¹ with a platinum plate as the working electrode, a silver wire as the pseudo-reference electrode, and a platinum wire as the counter electrode. The supporting electrolyte was tetrabutylammonium hexafluorophosphate (0.1 M) and ferrocene was selected to determine the potential of the silver wire electrode. The solutions were bubbled with a constant nitrogen flow for 15 min before measurements. The film surface morphology was measured with AFM (Seiko Instruments, SPA-400).

4.2 Quantum chemical calculations

The molecular structures for the two compounds in their neutral, cationic and anionic states were optimized by DFT method using the B3LYP functional, which employs the gradient correction of the exchange functional with three parameters by Becke and the correlation functional by Lee et al. The 6-31G(d) basis set was applied to the studied compounds. The values of k⁺ and k⁻ were also calculated for the DFT-optimized structures by both B3LYP/6-31G(d) level. All calculations were carried out using the Gaussian 09 program.

4.2 Device fabrication and performance measurements

In a general procedure, indium-tin oxide (ITO)-coated glass substrates were pre-cleaned and treated with UV ozone. The poly(ethylenedioxythiophene):poly(styrenesulfonate)(PEDOT:PSS) aqueous solution was pin-coated onto the ITO substrate and baked at 200 °C for 10 min under vacuum. The substrates were then taken into a nitrogen glove box, where the emission layer of host doped with Ir(mppy)₃ was spin-coated onto the PEDOT:PSS layer from 1,2-dichloroethane solution and annealed 80 °C for 30 min. The substrate was then transferred into an evaporation chamber, where the TPBI was evaporated at an evaporation rate of 1-2 Å s⁻¹ under a pressure of 4 × 10⁻⁴ Pa and the Cs₂CO₃/Al bilayer cathode was evaporated at evaporation rates of 0.2 and 10 Å s⁻¹ for Cs₂CO₃ and Al, respectively, under a pressure of 1 × 10⁻³ Pa. For hole-only devices, the host layer was spin-cast on PEDOT-modified ITO glass, and then Al electrode was deposited. For preparing electron-only devices, the host layer was directly spin-coated on ITO glass, and then Cs₂CO₃/Al electrodes were thermally deposited. The current-voltage-brightness characteristics of the devices were characterized with Keithley 4200 semiconductor characterization system. The electroluminescent spectra were collected with a Photo Research PR705 Spectrophotometer. All measurements of the device were carried out in ambient atmosphere without further encapsulations.

4.2 Materials

All manipulations involving air-sensitive reagents were performed under a dry nitrogen atmosphere.

9,9'-(5-(1-phenyl-1H-benzo[d]imidazol-2-yl)-1,3-phenylene) bis(3,6-di-tert-butyl-9H-carbazole) (2Cz-PBI)

A mixture of 2Br-PBI (0.85 g, 2 mmol), compound 1 (1.4 g, 5 mmol), CuI (0.01 g, 5 mmol), 1, 10-phenanthroline (0.01 g, 5 mmol), K₂CO₃ (1.4 g, 10 mmol), and dried DMF 50 mL was refluxed under an argon atmosphere for 24 h. After cooling to room temperature, the solvent was removed under vacuum and the residue was extracted with dichloromethane. The product was then obtained by column chromatography on silica gel with petroleum ether/ethyl acetate (5:1) as the eluent, to yield a white solid (0.8 g, 50%). ¹H-NMR (300 MHz, CDCl₃, δ): 8.10 (s, 4H), 7.94 (s, 1H), 7.89 (s, 2H), 7.83 (s, 1H), 7.67 (s, 3H), 7.47 (d, J = 12.5 Hz, 2H), 7.42 (d, J = 8.6 Hz, 4H), 7.37 - 7.26 (m, 2H), 7.23 (d, J = 8.4 Hz, 5H), 1.46 (s, 36H). ¹³C-NMR (75 MHz, CDCl₃, δ): 146.05, 142.61, 141.21, 133.19, 131.62, 130.23, 128.09, 127.58, 126.47, 126.30, 118.87, 113.32, 111.75, 37.33, 34.56. MS (MALDI-TOF) [m/z]: calcd for C₅₉H₆₀N₄, 825.1; found, 825.0. Anal. Calcd. for C₅₉H₆₀N₄: C, 85.88; H, 7.33; N 6.79. Found: C, 85.82; H, 7.22; N 6.65.

3,6-bis(3,6-di-tert-butyl-9H-carbazole-9yl)-9-(3-(1-phenyl-1H-benzo[d]imidazol-2-yl)phenyl)-9H-carbazole (4Cz-PBI)

This compound was prepared according to the procedure for the synthesis of 2Cz-PBI, with a yield of 48%. ¹H-NMR (300 MHz, CDCl₃, δ): 8.25 (s, 2H), 8.19 (s, 4H), 8.08 (d, J = 8.0 Hz, 4H), 8.03 (s, 2H), 7.71 (s, 3H), 7.55 (d, J = 8.2 Hz, 4H), 7.47 (d, J = 7.5 Hz, 11H), 7.33 (d, J = 8.5 Hz, 8H), 1.48 (s, 36H). ¹³C-NMR (75 MHz, CDCl₃, δ): 145.21, 143.52, 142.76, 142.36, 141.68, 140.33, 135.85, 133.80, 133.43, 130.31, 129.64, 129.33, 128.28, 127.45, 126.15, 126.02, 125.74, 123.77, 123.31, 121.85, 118.85, 113.58, 113.25, 112.72, 112.59, 111.70, 37.34, 34.66. MS (MALDI-TOF) [m/z]: calcd for C₈₃H₇₄N₆, 1155.5; found, 1155.2. Anal. Calcd. for C₈₃H₇₄N₆: C, 86.27; H, 6.45; N 7.27. Found: C, 86.23; H, 6.45; N 7.16.

9,9'-(5-(1-phenyl-1H-benzo[d]imidazol-2-yl)-1,3-phenylene) bis(3,6-bis(3,6-di-tert-butyl-9H-carbazole-9yl)-9H-carbazole) (6Cz-PBI)

This compound was prepared according to the procedure for the synthesis of Cz-4PBI, with a yield of 46%. ¹H-NMR (300 MHz, CDCl₃, δ): 8.25 (s, 5H), 8.16 (s, 9H), 7.78 (d, J = 7.1 Hz, 3H), 7.68 (d, J = 15.1 Hz, 11H), 7.47 (d, J = 8.6 Hz, 10H), 7.34 (d, J = 8.6 Hz, 10H), 1.46 (s, 72H). ¹³C-NMR (75 MHz, CDCl₃, δ): 138.11, 131.57, 131.15, 130.82, 127.88, 123.44, 122.11, 117.29, 116.08, 114.41, 109.44, 108.84, 34.55, 33.85, 31.84, 29.66. MS (MALDI-TOF) [m/z]: calcd for C₁₂₃H₁₂₀N₈, 1710.3; found, 1711.2. Anal. Calcd. for C₁₂₃H₁₂₀N₈: C, 86.38; H, 7.07; N 6.55. Found: C, 86.42; H, 7.03; N 6.49.

3-(3,5-bis(1-phenyl-1H-benzo[d]imidazol-2-yl)phenyl)-9-phenyl-9H-carbazole (Cz-2PBI).

Compound 4 (0.32 g, 1.0 mmol), DOB-2PBI (0.70 g, 1.2 mmol), and Tris(dibenzylideneacetone) dipalladium (0) (0.14 g, 0.15 mmol) were added to a round-bottomed flask equipped with a reflux condenser and dissolved in 50 mL of 1,4-dioxane. After adding 10 mL of aqueous 2 N potassium phosphate solution, the reaction mixture was heated at 110 °C for 24 h. The cooled crude mixture was poured into water and extracted with dichloromethane and dried over MgSO₄, filtered, and evaporated to yield a crude product. Flash column chromatography using CHCl₃ followed by reprecipitation with methanol and THF gave a product (0.38 g, 55%). ¹H-NMR (300 MHz, CDCl₃, δ): 8.14 (d, J = 7.6 Hz, 1H), 8.06 (s, 1H), 7.93 (d, J = 7.8 Hz, 2H), 7.80 (s, 3H), 7.69 - 7.48 (m, 11H), 7.36 (ddd, J = 18.2, 14.6, 7.4 Hz, 14H), 7.12 (d, J = 8.3 Hz, 1H). ¹³C-NMR (75 MHz, CDCl₃, δ): 135.84, 133.66, 133.05, 132.71, 132.54, 132.17, 132.00, 131.54, 131.24, 131.05, 130.26, 129.76, 129.70, 128.86, 127.77, 126.49, 126.43, 126.24, 126.03, 122.96, 122.81, 122.57, 122.40, 121.56, 114.19, 113.20, 112.58. MS (MALDI-TOF) [m/z]: calcd for C₅₀H₃₃N₅, 703.8; found, 703.2. Anal. Calcd. for C₅₀H₃₃N₅: C, 85.32; H, 4.73; N 9.95. Found: C, 82.45; H, 4.65; N 9.82.

3,6-bis(3,5-bis(1-phenyl-1H-benzo[d]imidazol-2-yl)phenyl)-9-phenyl-9H-carbazole (Cz-4PBI).

This compound was prepared according to the procedure for the synthesis of Cz-2PBI, with a yield of 58%. ¹H-NMR (300 MHz, CDCl₃, δ): 8.06 (s, 4H), 7.98 (s, 2H), 7.90 (d, J = 7.8 Hz, 4H), 7.83 (s, 2H), 7.59 (tp, J = 15.7, 7.9 Hz, 18H), 7.33 (ddd, J = 24.2, 11.4, 7.0 Hz, 23H). ¹³C-NMR (75 MHz, CDCl₃, δ): 139.92, 134.29, 133.37, 132.77, 132.63, 132.04, 132.01, 131.65, 131.26, 130.98, 130.70, 130.39, 130.17, 129.62, 129.14, 128.04, 126.46, 126.27, 125.88, 122.47, 121.41, 117.19, 113.18, 112.83, 112.74. MS (MALDI-TOF) [m/z]: calcd for C₈₂H₅₃N₉, 1164.3;

found, 1643.8. Anal. Calcd. for C₈₂H₅₃N₉: C, 84.59; H, 4.95; N 10.83. Found: C, 84.52; H, 4.82; N 10.65.

9-(3',5'-bis(1-phenyl-1H-benzo[d]imidazol-2-yl)biphenyl-4-yl)-3,6-bis(3,5-bis(1-phenyl-1H-benzo[d]imidazol-2-yl)phenyl)-9H-carbazole (Cz-6PBI)

This compound was prepared according to the procedure for the synthesis of Cz-4PBI, with a yield of 45%. ¹H-NMR (300 MHz, CDCl₃, δ): 8.07 (s, 4H), 7.99 (s, 2H), 7.97 - 7.86 (m, 9H), 7.84 (s, 2H), 7.62 (d, J = 3.3 Hz, 13H), 7.56 (t, J = 8.3 Hz, 8H), 7.48 - 7.27 (m, 35H). ¹³C-NMR (75 MHz, CDCl₃, δ): 140.92, 136.88, 136.47, 131.69, 130.19, 129.62, 129.18, 128.63, 128.18, 127.50, 127.12, 125.60, 123.92, 123.82, 123.49, 119.62, 118.76, 117.18, 110.62, 110.52, 110.30. MS (MALDI-TOF) [m/z]: calcd for C₁₁₄H₇₃N₁₃, 1624.9; found, 1624.2. Anal. Calcd. for C₁₁₄H₇₃N₁₃: C, 84.27; H, 4.35; N 11.21. Found: C, 84.23; H, 4.32; N 11.25.

Acknowledgements

We are grateful for the grants from the National Basic Research Program China (2013CB932902), National Natural Science Foundation of China (51103023, 21173042). We also thank for the support of the Scientific Research Foundation of Graduate School of Southeast University.

References

- [1] a) M. A. Baldo, D. F. O'Brien, Y. You, A. Shoustikov, S. Sibley, M. E. Thompson and S. R. Forrest, *Nature*, 1998, **395**, 151-154; b) H. Sasabe and J. Kido, *Eur. J. Org. Chem.*, 2013, **34**, 7653-7663; c) A. Chaskar, H. F. Chen and K. T. Wong, *Adv. Mater.*, 2011, **23**, 3876-3895.
- [2] a) C. M. Han, L. P. Zhu, J. Li, F. C. Zhao, H. Xu, D. G. Ma and P. F. Yan, *Chem.-Eur. J.*, 2014, **20**, 16350-16359; b) C. Han, Z. Zhang, H. Xu, J. Li, G. Xie, R. Chen, Y. Zhao and W. Huang, *Angew. Chem. Int. Ed.*, 2012, **51**, 10104-10108. c) Y. Tao, J. Xiao, C. Zheng, Z. Zhang, M. Yan, R. Chen, X. Zhou, H. Li, Z. An, Z. Wang, H. Xu and W. Huang, *Angew. Chem. Int. Ed.*, 2013, **52**, 10491-10495; d) C. Han, L. Zhu, J. Li, F. Zhao, Z. Zhang, H. Xu, Z. Deng, D. Ma and P. Yan, *Adv. Mater.*, 2014, **26**, 7070-7077; e) D. Yu, F. Zhao, C. Han, H. Xu, J. Li, Z. Zhang, Z. Deng, D. Ma and P. Yan, *Adv. Mater.*, 2012, **24**, 509-514.
- [3] a) J. Y. Li, T. Zhang, Y. J. Liang and R. X. Yang, *Adv. Funct. Mater.*, 2013, **23**, 619-628; b) J. Q. Ding, B. H. Zhang, J. H. Lu, Z. Y. Xie, L. X. Wang, X. B. Jing and F. S. Wang, *Adv. Mater.*, 2009, **21**, 4983-4986; c) M. C. Gather, A. Kohonen, A. Falcou, H. Becker and K. Meerholz, *Adv. Funct. Mater.*, 2007, **17**, 191-200; d) C. D. Muller, A. Falcou, N. Reckefuss, M. Rojahn, V. Wiederhirn, P. Rudati, H. Frohne, O. Nuyken, H. Becker and K. Meerholz, *Nature*, 2003, **421**, 829-833.
- [4] a) T. Chiba, Y. J. Pu, M. Hirasawa, A. Masuhara, H. Sasabe and J. Kido, *ACS Appl. Mater. Interfaces*, 2012, **4**, 6104-6108; b) T. Chiba, Y. J. Pu, H. Sasabe, J. Kido and Y. Yang, *J. Mater. Chem.*, 2012, **22**, 22769-22773; c) S. J. Su, D. Tanaka, Y. J. Li, H. Sasabe, T. Takeda and J. Kido, *Org. Lett.*, 2008, **10**, 941-944; d) N. Aizawa, Y. J. Pu, H. Sasabe and J. Kido, *Org. Electron.*, 2012, **13**, 2235-2242; e) N. Aizawa, Y. J. Pu, H. Sasabe and J. Kido, *Org. Electron.*, 2013, **14**, 1614-1620; f) C. C. Fan, M. H. Huang, W. C. Lin, H. W. Lin, Y. Chi, H. F. Meng, T. C. Chao and M. R. Tseng, *Org. Electron.*, 2014, **15**,

- 517-523; g) Y. H. Lin, Y. F. Chang, H. F. Meng, H. W. Zan, W. Y. Hsu and C. H. Chen, *Org. Electron.*, 2013, **14**, 3052-3060.
- [5] a) G. Liaptsis, D. Hertel and K. Meerholz, *Angew. Chem. Int. Ed.*, 2013, **52**, 9563-9567; b) G. Liaptsis and K. Meerholz, *Adv. Funct. Mater.*, 2013, **23**, 359-365; c) A. Kohnen, N. Riegel, J. Kremer, H. Lademann, D. C. Muller and K. Meerholz, *Adv. Mater.*, 2009, **21**, 879-883; d) T. L. Ye, S. Y. Shao, J. S. Chen, L. X. Wang and D. G. Ma, *ACS Appl. Mater. Interfaces*, 2011, **3**, 410-416. e) D. VASE analysis Yokoyama, Y. Setoguchi, A. Sakaguchi, M. Suzuki and C. Adachi, *Adv. Funct. Mater.*, 2010, **20**, 386-391; f) D. Yokoyama, H. Sasabe, Y. Furukawa, C. Adachi and J. Kido, *Adv. Funct. Mater.*, 2011, **21**, 1375-1382.
- [6] a) S. Feng, L. Duan, L. D. Hou, J. Qiao, D. Q. Zhang, G. F. Dong, L. D. Wang and Y. Qiu, *J. Phys. Chem. C*, 2011, **115**, 14278-14284; b) T. W. Lee, T. Noh, H. W. Shin, O. Kwon, J. J. Park, B. K. Choi, M. S. Kim, D. W. Shin and Y. R. Kim, *Adv. Funct. Mater.*, 2009, **19**, 1625-1630; c) C. Li, L. Duan, Y. Sun, H. Li and Y. Qiu, *J. Phys. Chem. C*, 2012, **116**, 19748-19754; d) F. Nuesch, D. Berner, E. Tutis, M. Schaer, C. Ma, X. Wang, B. Zhang and L. Zuppiroli, *Adv. Funct. Mater.*, 2005, **15**, 323-330; e) Q. Wang, C.-L. Ho, Y. Zhao, D. Ma, W.-Y. Wong and L. Wang, *Org. Electron.*, 2010, **11**, 238-246; f) C. W. Seo, J. H. Yoon and J. Y. Lee, *Org. Electron.*, 2012, **13**, 341-349; g) J.-h. Yoon and I.-s. Park, *Appl. Phys. Lett.*, 2008, **93**, 193303.
- [7] a) Y. T. Chang, J. K. Chang, Y. T. Lee, P. S. Wang, J. L. Wu, C. C. Hsu, I. W. Wu, W. H. Tseng, T. W. Pi, C. T. Chen and C. I. Wu, *ACS Appl. Mater. Interfaces*, 2013, **5**, 10614-10622; b) X. H. Yang and D. Neher, *Appl. Phys. Lett.*, 2004, **84**, 2476; c) S. Gong, Y.-L. Chang, K. Wu, R. White, Z.-H. Lu, D. Song and C. Yang, *Chem. Mat.*, 2014, **26**, 1463-1470; d) K. S. Yook, S. E. Jang, S. O. Jeon and J. Y. Lee, *Adv. Mater.*, 2010, **22**, 4479-4483; e) C. Liu, Y. H. Li, Y. F. Li, C. L. Yang, H. B. Wu, J. G. Qin and Y. Cao, *Chem. Mat.*, 2013, **25**, 3320-3327; f) W. Jiang, H. G. Xu, X. X. Ban, G. L. Yuan, Y. M. Sun, B. Huang, L. Duan and Y. Qiu, *Org. Lett.*, 2014, **16**, 1140-1143.
- [8] a) K. S. Yook and J. Y. Lee, *Adv. Mater.*, 2014, **26**, 4218-4233; b) X. H. Zhu, J. B. Peng, Y. Cao and J. Roncali, *Chem. Soc. Rev.*, 2011, **40**, 3509-3524; c) L. A. Duan, L. D. Hou, T. W. Lee, J. A. Qiao, D. Q. Zhang, G. F. Dong, L. D. Wang and Y. Qiu, *J. Mater. Chem.*, 2010, **20**, 6392-6407; d) Y. J. Pu, T. Chiba, N. Aizawa, H. Sasabe and J. Kido, *J. Photopolym. Sci. Technol.*, 2013, **26**, 403-410; e) P. I. Shih, Y. H. Tseng, F. I. Wu, A. K. Dixit and C. F. Shu, *Adv. Funct. Mater.*, 2006, **16**, 1582-1589; f) L. X. Xiao, X. Xing, Z. J. Chen, B. Qu, H. L. Lan, Q. H. Gong and J. Kido, *Adv. Funct. Mater.*, 2013, **23**, 1323-1330.
- [9] a) E. Mondal, W. Y. Hung, H. C. Dai and K. T. Wong, *Adv. Funct. Mater.*, 2013, **23**, 3096-3105; b) C. W. Lee and J. Y. Lee, *Chem. Commun.*, 2013, **49**, 1446-1448; c) Z. Zhang, Z. Zhang, R. Chen, J. Jia, C. Han, C. Zheng, H. Xu, D. Yu, Y. Zhao, P. Yan, S. Liu and W. Huang, *Chem.-Eur. J.*, 2013, **19**, 9549-9561; d) E. Mondal, W. Y. Hung, Y. H. Chen, M. H. Cheng and K. T. Wong, *Chem.-Eur. J.*, 2013, **19**, 10563-10572; e) H. Sasabe, H. Nakanishi, Y. Watanabe, S. Yano, M. Hirasawa, Y. J. Pu and J. Kido, *Adv. Funct. Mater.*, 2013, **23**, 5550-5555; f) S. J. Su, Y. Takahashi, T. Chiba, T. Takeda and J. Kido, *Adv. Funct. Mater.*, 2009, **19**, 1260-1267; g) Q. S. Zhang, T. Komino, S. P. Huang, S. Matsunami, K. Goushi and C. Adachi, *Adv. Funct. Mater.*, 2012, **22**, 2327-2336; h) S. J. Su, H. Sasabe, Y. J. Pu, K. Nakayama and J. Kido, *Adv. Mater.*, 2010, **22**, 3311-3316; i) J. Wu, Y. Liao, S. X. Wu, H. B. Li and Z. M. Su, *Phys. Chem. Chem. Phys.*, 2012, **14**, 1685-1693; j) D. Kim, L. Zhu and J.-L. Brédas, *Chem. Mater.*, 2012, **24**, 2604-2610; k) Z. Ge, T. Hayakawa, S. Ando, M. Ueda, T. Akiike, H. Miyamoto, T. Kajita and M. A. Kakimoto, *Chem. Mater.*, 2008, **20**, 2532-2537.
- [10] a) H. Sasabe, N. Toyota, H. Nakanishi, T. Ishizaka, Y. J. Pu and J. Kido, *Adv. Mater.*, 2012, **24**, 3212-3217; b) C. Han, Z. Zhang, H. Xu, S. Yue, J. Li, P. Yan, Z. Deng, Y. Zhao, P. Yan and S. Liu, *J. Am. Chem. Soc.*, 2012, **134**, 19179-19188; c) J. Zhao, G.-H. Xie, C.-R. Yin, L.-H. Xie, C.-M. Han, R.-F. Chen, H. Xu, M.-D. Yi, Z.-P. Deng, S.-F. Chen, Y. Zhao, S.-Y. Liu and W. Huang, *Chem. Mater.*, 2011, **23**, 5331-5339; d) C. Han, Z. Zhang, H. Xu, G. Xie, J. Li, Y. Zhao, Z. Deng, S. Liu and P. Yan, *Chem.-Eur. J.*, 2013, **19**, 141-154.
- [11] a) S. J. Su, H. Sasabe, T. Takeda and J. Kido, *Chem. Mater.*, 2008, **20**, 1691-1693; b) S. J. Su, C. Cai and J. Kido, *Chem. Mater.*, 2011, **23**, 274-284; c) S.-J. Su, C. Cai, J. Takamatsu and J. Kido, *Org. Electron.*, 2012, **13**, 1937-1947; d) S. J. Su, E. Gonmori, H. Sasabe and J. Kido, *Adv. Mater.*, 2008, **20**, 4189-4194; e) S. J. Su, C. Cai and J. Kido, *J. Mater. Chem.*, 2012, **22**, 3447-3456.
- [12] a) B. Pan, H. Huang, X. Yang, J. Jin, S. Zhuang, G. Mu and L. Wang, *J. Mater. Chem. C*, 2014, **2**, 7428; b) L. A. Duan, J. A. Qiao, Y. D. Sun and Y. Qiu, *Adv. Mater.*, 2011, **23**, 1137-1144; c) J. Zou, H. Wu, C. S. Lam, C. Wang, J. Zhu, C. Zhong, S. Hu, C. L. Ho, G. J. Zhou, H. Wu, W. C. Choy, J. Peng, Y. Cao and W. Y. Wong, *Adv. Mater.*, 2011, **23**, 2976-2980; d) Y. T. Tao, Q. Wang, C. L. Yang, Q. Wang, Z. Q. Zhang, T. T. Zou, J. G. Qin and D. G. Ma, *Angew. Chem. Int. Ed.*, 2008, **47**, 8104-8107; e) T. Earmme and S. A. Jenekhe, *Adv. Funct. Mater.*, 2012, **22**, 5126-5136; f) H. Sasabe and J. Kido, *J. Mater. Chem. C*, 2013, **1**, 1699-1707; g) N. Aizawa, Y. J. Pu, H. Sasabe and J. Kido, *Org. Electron.*, 2013, **14**, 1614-1620; h) M. Debeaux, M. W. Thesen, D. Schneidenbach, H. Hopf, S. Janietz, H. Kruger, A. Wedel, W. Kowalsky and H. H. Johannes, *Adv. Funct. Mater.*, 2010, **20**, 399-408.
- [13] a) W. Jiang, L. Duan, J. Qiao, G. F. Dong, L. D. Wang and Y. Qiu, *Org. Lett.*, 2011, **13**, 3146-3149; b) W. Jiang, J. Tang, X. Ban, Y. Sun, L. Duan and Y. Qiu, *Org. Lett.*, 2014, **16**, 5346-5349; c) W. Jiang, L. A. Duan, J. Qiao, D. Q. Zhang, G. F. Dong, L. D. Wang and Y. Qiu, *J. Mater. Chem.*, 2010, **20**, 6131-6137; d) W. Jiang, L. A. Duan, J. A. Qiao, G. F. Dong, D. Q. Zhang, L. D. Wang and Y. Qiu, *J. Mater. Chem.*, 2011, **21**, 4918-4926.
- [14] Z. A. Li, Y. Q. Liu, G. Yu, Y. G. Wen, Y. L. Guo, L. Ji, J. G. Qin and Z. Li, *Adv. Funct. Mater.*, 2009, **19**, 2677-2683.
- [15] a) L. Wang, Y. Wu, G.-G. Shan, Y. Geng, J.-Z. Zhang, D.-M. Wang, G.-C. Yang and Z.-M. Su, *J. Mater. Chem. C*, 2014, **2**, 2859; b) L. Duan, J. Qiao, Y. Sun and Y. Qiu, *Adv. Mater.*, 2011, **23**, 1137-1144; c) P. J. Low, M. A. J. Paterson, D. S. Yufit, J. A. K. Howard, J. C. Cherryman, D. R. Tackley, R. Brook and B. Brown, *J. Mater. Chem.*, 2005, **15**, 2304-2315.
- [16] a) T. Yamada, F. Suzuki, A. Goto, T. Sato, K. Tanaka and H. Kaji, *Org. Electron.*, 2011, **12**, 169-178; b) C. Lee, R. Waterland and K. Sohlberg, *J. Chem. Theory Comput.*, 2011, **7**, 2556-2567; c) H. Li, L. Duan, D. Zhang and Y. Qiu, *J. Phys. Chem. C*, 2014, **118**, 14848-14852; d) J.-H. Pan, Y.-M. Chou, H.-L. Chiu and B.-C. Wang, *J. Phys. Org. Chem.*, 2007, **20**, 743-753.

Notes

^a School of Chemistry and Chemical Engineering, Southeast University, Nanjing, Jiangsu, P. R. China 211189, E-mail: jiangw@seu.edu.cn

^b Department of Chemistry, Tsinghua University, Beijing 100084, P.R. China, E-mail: duanl@mail.tsinghua.edu.cn

Electronic Supplementary Information (ESI) available. See DOI: 10.1039/b000000x/

Suffering the solvent impurities and oxygen diffusion induced strong electron trapping effect, the balanced charge transporting behaviors seems more important than the extremely small ΔE_{ST} in the solution-processed devices.

